

The PHOENIX Exoplanet Retrieval Algorithm and Using H⁻ Opacity as a Probe in Ultra-hot Jupiters

JOSHUA D. LOTHINGER^{1,2} AND TRAVIS S. BARMAN²

¹*Department of Physics and Astronomy, Johns Hopkins University, Baltimore, MD, USA*

²*Lunar and Planetary Laboratory, University of Arizona, Tucson, AZ, USA*

(Dated: May 8, 2020)

ABSTRACT

Atmospheric retrievals are now a standard tool to analyze observations of exoplanet atmospheres. This data-driven approach quantitatively compares atmospheric models to observations in order to estimate atmospheric properties and their uncertainties. In this paper, we introduce a new retrieval package, the PHOENIX Exoplanet Retrieval Analysis (PETRA). PETRA places the PHOENIX atmosphere model in a retrieval framework, allowing us to combine the strengths of a well-tested and widely-used atmosphere model with the advantages of retrieval algorithms. We validate PETRA by retrieving on simulated data for which the true atmospheric state is known. We also show that PETRA can successfully reproduce results from previously published retrievals of WASP-43b and HD 209458b. For the WASP-43b results, we show the effect that different line lists and line profile treatments have on the retrieved atmospheric properties. Lastly, we describe a novel technique for retrieving the temperature structure and e^- density in ultra-hot Jupiters using H⁻ opacity, allowing us to probe atmospheres devoid of most molecular features with JWST.

Keywords: planets and satellites: atmospheres, methods: numerical

1. INTRODUCTION

Retrieval algorithms are now widely-used to infer atmospheric properties, like the composition and temperature structure, from observations of sub-stellar objects. Retrieval algorithms have two basic parts: a forward model that produces a spectrum and a statistical framework that chooses parameters for that forward model and compares the spectra with observations. A primary advantage of using retrieval algorithms over grid-based searches is that retrievals provide robust estimations of parameter uncertainties, correlations, and degeneracies through efficient sampling of parameter space and the posterior distribution. While retrieval forward models are generally not fully self-consistent and require multiple parameterizations and assumptions for the sake of computational efficiency, retrievals are a valuable method to interpret observations.

Retrievals have been used to analyze transit (e.g., [Line et al. 2012](#); [Benneke & Seager 2012](#); [Waldmann et al.](#)

[2015](#); [Barstow et al. 2017](#); [MacDonald & Madhusudhan 2017](#); [Howe et al. 2017](#); [Mollière et al. 2019](#)) and secondary-eclipse observations (e.g., [Line et al. 2014b](#); [Gandhi & Madhusudhan 2018](#); [Waldmann et al. 2015](#); [Evans et al. 2017](#); [Mollière et al. 2019](#); [Kitzmann et al. 2020](#); [Himes et al. 2020](#)), as well as observations of self-luminous objects like directly-imaged exoplanets ([Lee et al. 2013](#); [Lavie et al. 2017](#); [Gravity Collaboration et al. 2020](#)) and brown dwarfs ([Line et al. 2015, 2017](#); [Burningham et al. 2017](#)). Recently, the application of retrieval algorithms to combine low- and high-resolution data has been explored ([Brogi et al. 2017](#); [Brogi et al. 2019](#); [Fisher et al. 2019](#); [Gandhi et al. 2019](#); [Gibson et al. 2020](#)). See [Madhusudhan \(2018\)](#) for an overview of many existing retrieval algorithms and [Barstow & Heng \(2020\)](#) for a discussion of open problems in retrieval analysis.

PHOENIX is a well-tested self-consistent atmosphere model that has been used to study the atmospheres of stellar and sub-stellar atmospheres for decades ([Hauschildt et al. 1997, 1999](#); [Allard et al. 2011](#); [Barman et al. 2001, 2011](#); [Lothringer et al. 2018](#); [Lothringer & Barman 2019](#)). In self-consistent frameworks, the model is typically iterated until certain convergence criteria

are met (i.e., radiative-convective equilibrium). Self-consistent models provide us with our best prediction of the structure and composition of an atmosphere based on the physical assumptions included in the model. The comparison of observations with self-consistent models can provide insight into the processes at work in the atmosphere.

In this work, we introduce a new retrieval framework, the PHOENIX Exoplanet Retrieval Algorithm (PETRA), which utilizes PHOENIX as its forward model. PETRA allows us to combine many of the strengths of one of the most widely-used atmosphere models with the advantages of retrieval algorithms. PETRA’s use of PHOENIX’s opacity database will prove useful in the identification and characterization of molecules and atoms in complex exoplanet atmospheres, as well as in understanding line list biases. PHOENIX’s line sampling methods will also be effective at retrieving atmospheric properties from high-spectral resolution observations. Additionally, PHOENIX’s broad applicability is advantageous in a retrieval forward model, as we will be able to use PETRA to explore exoplanet, brown dwarf, and stellar atmospheres in different geometries while being able to compare to self-consistent predictions from the same model.

Section 2 explains the structure of PETRA, as well as the parameterizations and statistical framework used. In Section 3, we validate PETRA by presenting retrievals on simulated data with known atmospheric parameters. We also compare PETRA to other retrieval tools by comparing results for WASP-43b and HD 209458b. Lastly, we demonstrate a novel use of PETRA to retrieve the temperature structure and e^- density in ultra-hot Jupiters from James Webb Space Telescope (JWST) simulated observations using H^- opacity in Section 4.

2. METHODS

2.1. The Forward Model

As mentioned above, the forward model uses a modified version of the atmosphere code PHOENIX. In its widely-used self-consistent version, PHOENIX is capable of modeling a variety of objects from cool, cloudy brown-dwarfs to dwarf and giant stars in both plane-parallel and spherically symmetric geometry. This breadth in applicability extends to PETRA as well. Figure 1 illustrates the basic structure of PETRA. The left-hand column represents the statistical framework, while the right-hand column shows the steps that utilize PHOENIX for calculating the spectrum.

One of the main motivations for developing PETRA is to utilize PHOENIX’s expansive opacity database

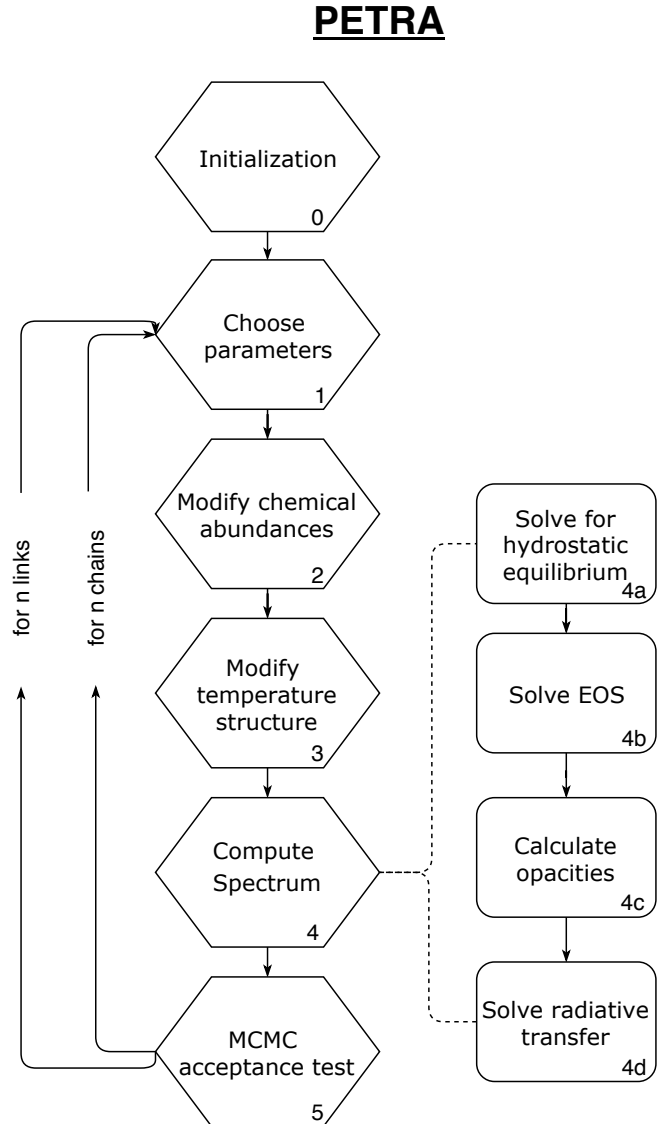


Figure 1. A flow chart illustrating the structure of PETRA. Boxes 4a-d represent the steps that directly utilize PHOENIX.

and opacity sampling routines. PHOENIX has molecular opacity information including many isotopologues, deuterated species, and multiple line lists. Comprehensive atomic line lists are used for elements from hydrogen to uranium, including many bound-free and continuous opacities. More information on the opacities used that are relevant to exoplanet modelling can be found in Lothringer et al. (2018) and Lothringer & Barman (2019). New line lists are currently being incorporated into PHOENIX and PETRA, including HITEMP H_2O and CO_2 (Rothman et al. 2010), AIO (Patrascu et al. 2015), TiO (McKemmish et al. 2019), and SH (Zahnle et al. 2009; Yurchenko et al. 2018).

PHOENIX uses direct opacity sampling (dOS) to calculate opacities. dOS operates by taking line list information and selecting all relevant lines above some flexible cutoff in opacity relative to the continuum. This is done at the beginning of each model run without the need for precomputed opacity tables, allowing a high degree of flexibility when it comes to changing model resolution, line lists, and included opacity sources. This flexibility will allow PETRA to retrieve quantities from high-resolution observations at high accuracy. For each iteration, the selected lines are broadened and the opacity is then sampled on a user-defined wavelength grid.

Within PHOENIX, line profiles can be calculated as Gaussian, Voigt, or special line profiles depending on the line’s strength. In all cases, the lines are broadened accounting for the natural line profile, quadratic Stark damping, Van der Waals damping, and thermal broadening. The linear Stark effect on atomic hydrogen lines is accounted for by using special line profiles. The Voigt profiles can be described as

$$V(u, a) = \frac{(\lambda^2/c)}{\pi^{1/2}\Delta\lambda_D} H(u, a) \quad (1)$$

with $u = \Delta\lambda/\Delta\lambda_D$ and $a = (\lambda^2\gamma/4\pi c)/\Delta\lambda_D$, where λ is the wavelength, $\Delta\lambda$ is the distance from the line center, $\Delta\lambda_D$ is the thermal broadening Gaussian width, and c is the speed of light (Gray 1992; Schweitzer et al. 1996). γ is the Lorentzian damping constant, which is the sum of the natural, quadratic Stark, and Van der Waals broadening widths. Lastly, $H(u, a)$ is the Hjerting function (Hjerting 1938), given by

$$H(u, a) = \frac{a}{\pi} \int_{-\infty}^{\infty} \frac{e^{-u'^2}}{(u - u')^2 + a^2} du'. \quad (2)$$

The calculation of the Voigt profile can be computationally expensive when done for many thousands of lines on the fly, so Gaussian profiles are sometimes assumed for weak lines. In Section 3.2.1, we test whether Gaussian profiles can be assumed within PETRA to speed up the calculation of the spectrum. Even with calculating Voigt profiles, PETRA can complete a single iteration modeling the CO bandhead from 2.3-2.7 μm at 0.1 \AA sampling ($R \sim 230,000, \sim 0.01\text{cm}^{-1}$) in about 2 seconds on a single 28-core node of a high-performance computer.

Chemical equilibrium is calculated with PHOENIX’s Astrophysical Chemical Equilibrium Solver (ACES) which we use to calculate the equation of state for 894 different species. In the PETRA retrievals shown below, the chemical abundances are read from a precomputed partial pressure table and then modified for the species treated as free parameters. PETRA is also capable of

retrieving abundances self-consistently, using quantities like the metallicity, elemental, or even isotopic ratios as free parameters.

2.1.1. Temperature Structure

In the retrieval of Earth, solar system, and brown dwarf atmospheric observations, there is generally enough data for the temperature structure to be determined layer-by-layer (e.g., Gottwald & Bovensmann 2011; Irwin et al. 2008; Line et al. 2014a). The low signal-to-noise nature of exoplanet atmosphere observations often necessitates reducing the number of free parameters as much as possible. It is therefore advantageous to parameterize the temperature structure.

In PETRA, we have incorporated n-layer models (where each layer is connected via a logarithmic temperature gradient), the parameterization of Madhusudhan & Seager (2009), and the parameterization used in Line et al. (2013). The latter is an analytic parametrization for atmospheres in radiative equilibrium using a three-channel Eddington approximation from Parmentier & Guillot (2014). Because of the physical motivation of this parameterization and its flexibility, we adopt it for this work.

2.1.2. Non-Uniform Vertical Abundances

In exoplanet atmosphere retrievals, vertical abundances are often assumed to be constant with pressure. This assumption can break down at high temperatures in ultra-hot Jupiters due to the thermal dissociation of molecules and at temperatures near the transition in chemical equilibrium between CH_4 and CO as the dominant carbon-bearing molecule. Within PETRA, the vertical abundances can be described by three parameters: η_{max} (the maximum volume mixing ratio (VMR) of the species), ϵ (the power of the slope), and η_0 (the abundance at $\log(P_{\text{cgs}})=0$ (i.e., $P = 1 \mu\text{bar} = 1 \text{barye}$)). The VMR is thus parameterized as:

$$\log_{10}(\text{VMR}) = \min(\eta_{\text{max}}, \epsilon * \log_{10}(P) + \eta_0). \quad (3)$$

For example, in a typical ultra-hot Jupiter undergoing molecular dissociation at pressures below 1 mbar, CO would have $\eta_{\text{max}} \sim -3.5$, $\eta_0 \sim -7$, and ϵ would be positive (the molecular abundance would be increasing with pressure). For species like ions that generally decrease with pressure at photospheric depths, ϵ would be negative.

This parameterization is clearly limited as there is no physical reason to assume a power-law slope. Future studies may explore layer-by-layer abundance retrievals. This parameterization, however, provides necessary flexibility and a fundamental insight into whether atmo-

spheric species are increasing or decrease with pressure, which will be important in Section 4.

2.2. MCMC/Statistical Framework

We utilize Differential Evolution Markov Chains (DEMC) (Ter Braak 2006) with “snooker” updates (ter Braak & Vrugt 2008) to explore the parameter space and build our posterior distributions. DEMC is a type of Markov Chain Monte Carlo (MCMC) that uses information from other chains to determine the next step’s size and direction, which is an improvement on the random direction and manual step size of traditional Metropolis-Hastings MCMC. DEMC has been tested and used for a number of exoplanet retrieval applications (Line et al. 2013; Evans et al. 2017).

We have also implemented a version of parallel tempering in PETRA. At the beginning of a retrieval when comparing the likelihoods of the current and proposed state, we raise each likelihood to a power, ζ , such that it is accepted with probability

$$p = \min \left(1, \frac{\pi(\theta')\mathcal{L}(\theta')^\zeta}{\pi(\theta)\mathcal{L}(\theta)^\zeta} \right), \quad (4)$$

where $\pi(\theta')$ is the prior on the proposed state, θ' , $\pi(\theta)$ is the prior on the current state, θ , $\mathcal{L}(\theta')$ is the likelihood of the proposed state, $\mathcal{L}(\theta)$ is the likelihood of the current state, θ , and ζ is the ‘temperature’, which we define from 0 to 1. $\zeta = 1$ corresponds to no tempering while $0 < \zeta < 1$ “flattens” posterior space. Flatter posterior distributions help the chains explore different local likelihood minima regions without getting stuck. We generally begin each retrieval with a short period of tempering where ζ begins at a minimum, ζ_{min} , usually between 0.5 and 0.9 and slowly rises for n_{max} iterations until $\zeta = 1$:

$$\zeta = (\zeta_{min} - 1) * \left(1 - \frac{n}{n_{max}} \right) + 1, \quad (5)$$

where n is the current iteration. We usually set n_{max} between 100 to 1,000 so tempering only occurs during the initial burn-in of the chains. Our choice of n_{max} helps ensure that we find the global likelihood maximum.

In a full retrieval using the temperature structure parameterization described above and four to eight molecular abundances as free parameters for a total of 9 to 13 free parameters, we use about 20 chains and can reach convergence, as indicated by a Gelman-Rubin statistic

< 1.01 (Gelman & Rubin 1992)¹, in $< 10^4$ iterations per chain.

In future work, we will incorporate nested sampling, which is a powerful method to do Bayesian model comparison (Skilling 2004). This is useful to determine if the complexity of the model, i.e., the number of free parameters, is justified.

3. TESTS

3.1. Simulated Data from PHOENIX

To validate the statistical framework of PETRA, we used our forward model to compute a hot Jupiter spectrum with parameters similar to those of WASP-43b. From this spectrum, we simulated observations from the *Hubble Space Telescope’s* Wide Field Camera 3 (HST/WFC3) and *Spitzer* Channels 1 and 2 using the bins and uncertainties from Kreidberg et al. (2015). We then retrieved the atmospheric parameters using PETRA from these simulated data for which we know the ‘true’ values. Our retrieval uses the same parameters as the input model: five parameters to describe the temperature profile (discussed above) and four parameters for the H₂O, CO, CO₂, and CH₄ abundances.

Figure 2 shows the simulated observations compared to the median retrieved spectrum and the spectrum’s 1- σ uncertainty region. PETRA is able to fit the simulated data well, with $\chi^2 = 17.23$ for the median retrieved spectrum. With 17 data points, we obtain a χ^2 per data point of 1.01, quite similar to the quality of fits obtained with real data in the sections below.

Figure 3 shows the retrieved constraints on the molecular abundances. The top plot in each column shows the 1-dimensional posterior distribution for each molecular abundance. Below the 1-dimensional posteriors are 2-dimensional posteriors showing how the estimates of each molecular abundance depend on the other molecular abundances. The retrieved molecular abundances agree to within 1- σ of the input molecular abundance, indicating that we are retrieving correct values.

Figure 4 compares the retrieved temperature structure constraints with the input temperature profile. The retrieved temperature structure is within 1 to 2- σ of the input temperature profile in the optical and IR photosphere region between 1-100 mbar. The upper atmosphere, above the optical and IR photosphere deviates from the input temperature profile, but since none of the simulated observation probe this region, this is acceptable. Retrieved information about atmospheric depths

¹ In the simplest terms, the Gelman-Rubin statistic compares the standard deviation of each chain with the standard deviation of the mean of the chains.

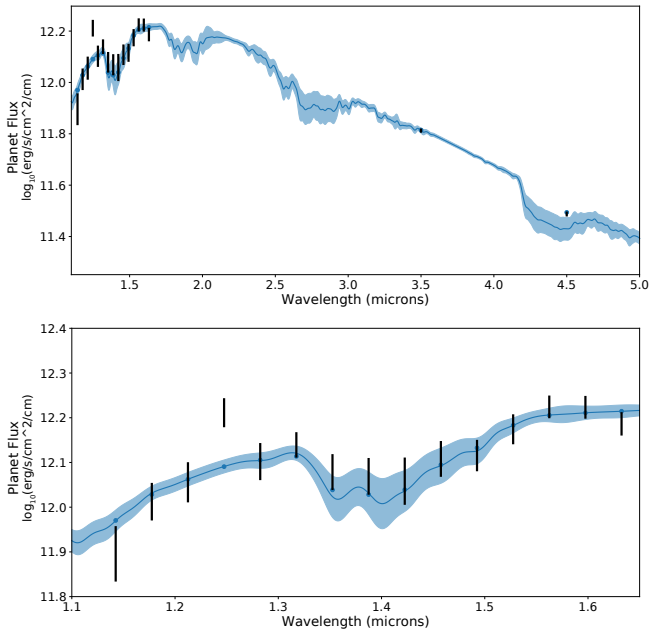


Figure 2. Simulated observations of a generic hot Jupiter similar to WASP-43b from a PHOENIX forward model compared to the retrieved median spectrum and $1\text{-}\sigma$ uncertainty region. The bottom figure is a zoomed in version of the top, highlighting the 1.4 micron H_2O feature from HST/WFC3 observations. The region between the end of the HST/WFC3 bandpass ($\sim 1.7\ \mu\text{m}$) and the beginning of the *Spitzer* Channel 1 bandpass ($\sim 3\ \mu\text{m}$) was sampled sparsely for computational efficiency.

not probed by the observations is often biased by the parameterization of the temperature profile and, thus, do not provide reliable constraints.

The region being probed by the observations can also be understood by looking at the contribution functions of the atmosphere at wavelengths corresponding to the observations. Figure 5 shows contribution functions at HST/WFC3 wavelengths inside and outside the H_2O absorption feature, as well as the two *Spitzer* photometry points. The peak of each contribution function shows from which pressure most of the flux at a given wavelength is radiated. While the HST/WFC3 continuum probes deep in the atmosphere at around 100 mbar, the other wavelengths probe higher up the atmosphere (due to increased opacity at these wavelengths) at around 5 mbar. Therefore, the WASP-43b’s temperature is only constrained by the observations between about 1 and 100 mbar.

3.2. Comparison to Previous Retrievals

3.2.1. WASP-43b

In order to compare PETRA with other retrieval suites, we retrieved the temperature profile and molec-

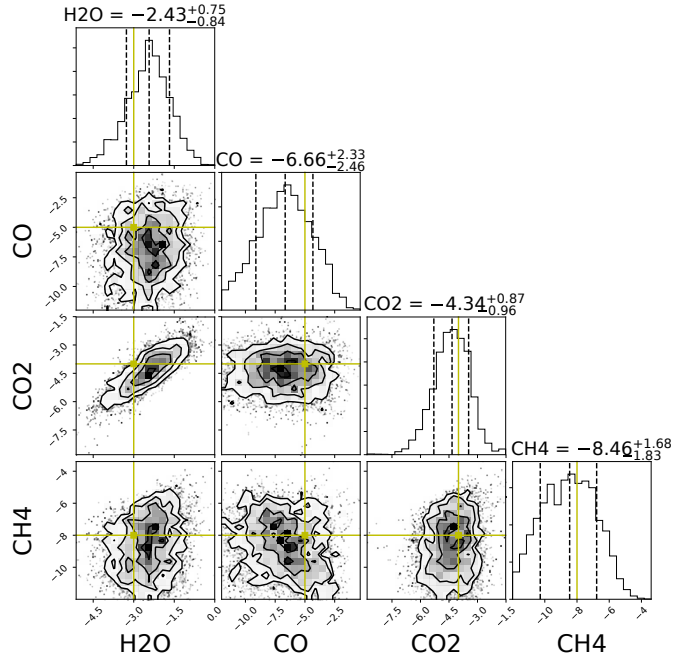


Figure 3. Plot of the posterior distributions of molecular abundances from the WASP-43b simulated data test. The top-most plot of each column shows the 1-D posterior for each molecular abundance included in the test. The middle dotted line shows the average retrieved value, while the dotted lines to each side bound the $1\text{-}\sigma$ uncertainty range. The yellow lines indicate the ‘true’ input value that generated the simulated data. Below the 1-D posteriors are the 2-D posterior distributions.

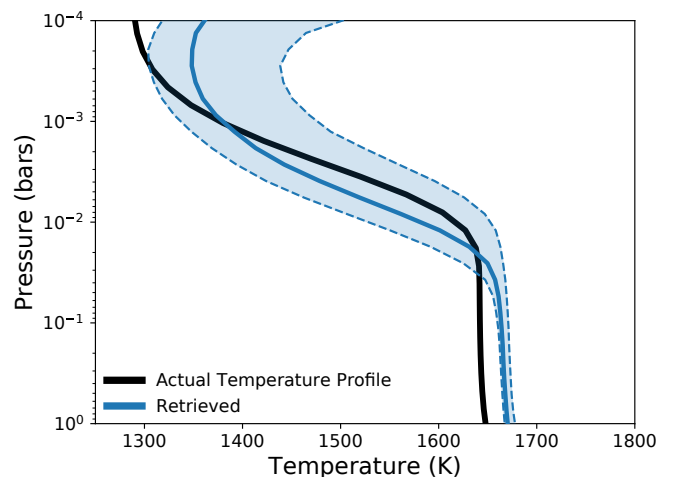


Figure 4. Comparison of the input temperature profile (gold) for the WASP-43b simulated data test compared to the average retrieved temperature profile (dashed black) and the $1\text{-}\sigma$ uncertainty region (shaded grey region). The region above 1 mbar is not probed by the observations and the constraints shown are an outcome of the parameterization.

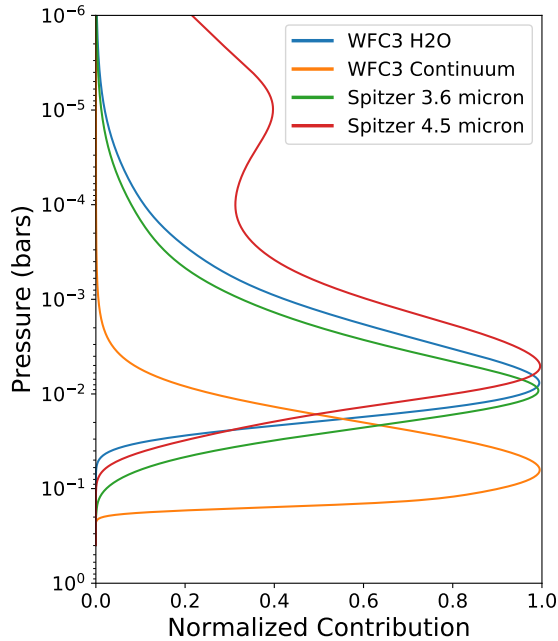


Figure 5. Contribution functions for WASP-43b’s dayside atmosphere at 1.25, 1.4, 3.6, and 4.5 μm , corresponding to outside the 1.4 μm H₂O feature, inside the 1.4 μm H₂O feature, *Spitzer* channel 1, and *Spitzer* channel 2, respectively.

ular abundances of hot Jupiter WASP-43b using HST/WFC3 and *Spitzer* data from Kreidberg et al. (2014), which was analyzed with the CHIMERA retrieval suite (Line et al. 2013, 2014b). This same data was also analyzed in (Evans et al. 2017) with the ATMO retrieval suite. Both frameworks retrieved a non-inverted atmosphere with an approximately solar abundance of H₂O.

As was done in the CHIMERA retrievals, we use the temperature profile parameterization described above and fit for the H₂O, CO, CO₂, and CH₄ abundances. We analyzed the WASP-43b data with PETRA using two different H₂O line lists, BT2 (Barber-Tennyson): Barber et al. (2006) and HITRAN2008: Rothman et al. (2009). BT2 is a computed list of H₂O transition frequencies and intensities and comprises over 5×10^6 transitions. HITRAN2008 is a compilation of transitions from various sources, including over 6.9×10^4 H₂O transitions.

As mentioned in Section 2, the calculation of the Voigt profile can be computationally expensive when done on the fly as in PETRA. Additionally, (Barstow et al. 2020) showed that assumptions in line broadening can lead to significant differences in forward models and retrieval results. To understand the overall effect of the line profile shape on retrieval results and to test whether Gaus-

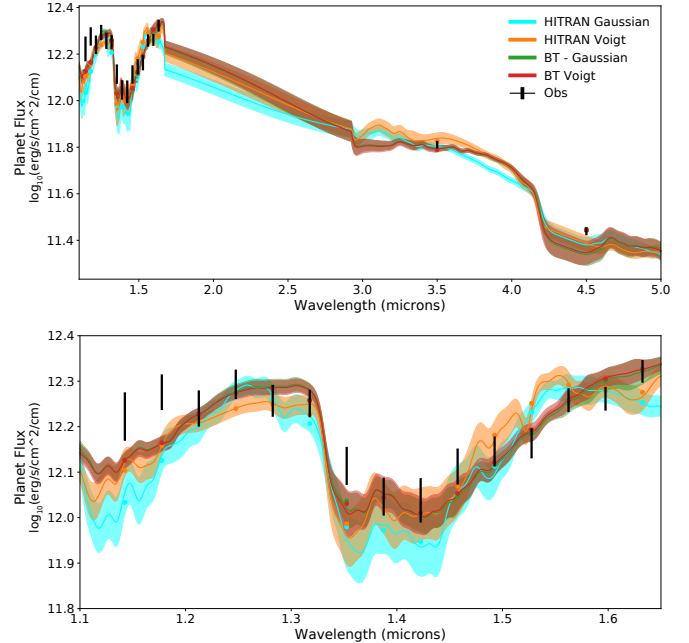


Figure 6. Observations of hot Jupiter WASP-43b from Kreidberg et al. (2015) compared to the retrieved median spectrum and 1- σ uncertainty region for retrievals using different H₂O line lists and line profile treatment (see text). The region between the end of the HST/WFC3 bandpass ($\sim 1.7 \mu\text{m}$) and the beginning of the *Spitzer* Channel 1 bandpass ($\sim 3 \mu\text{m}$) was sampled sparsely for computational efficiency.

sian profiles can provide physically accurate retrieved atmospheric properties, we ran retrievals with each list assuming Gaussian and then Voigt line profiles when calculating the opacities.

Figure 6 shows how the observations compare to the median retrieved spectra and 1- σ uncertainties for each retrieval. The agreement between the models and observations is quite similar for the two retrievals using the BT2 H₂O line list. The median spectrum retrieved using the BT2 list with Voigt line profiles has $\chi^2 = 17.39$, giving a χ^2 per data point of $\chi^2/17 = 1.023$. The median spectrum retrieved using the BT2 list with the Gaussian line profiles matches the data marginally better with $\chi^2 = 15.97$ and a χ^2 per data point of 0.939. Both of retrievals are comparable to the χ^2 per data point of 1.2 found with CHIMERA in Kreidberg et al. (2015).

The HITRAN2008 list provides a somewhat worse fit, with $\chi^2 = 31.54$ and a χ^2 per data point of 1.86 using Gaussian profiles and with $\chi^2 = 39.16$ and a χ^2 per data point of 2.3 using Voigt profiles. This may provide some evidence that the BT2 list is more capable of producing hot Jupiter spectra that better match observations. This is expected since the BT2 list is constructed with special attention paid to the high temperatures found

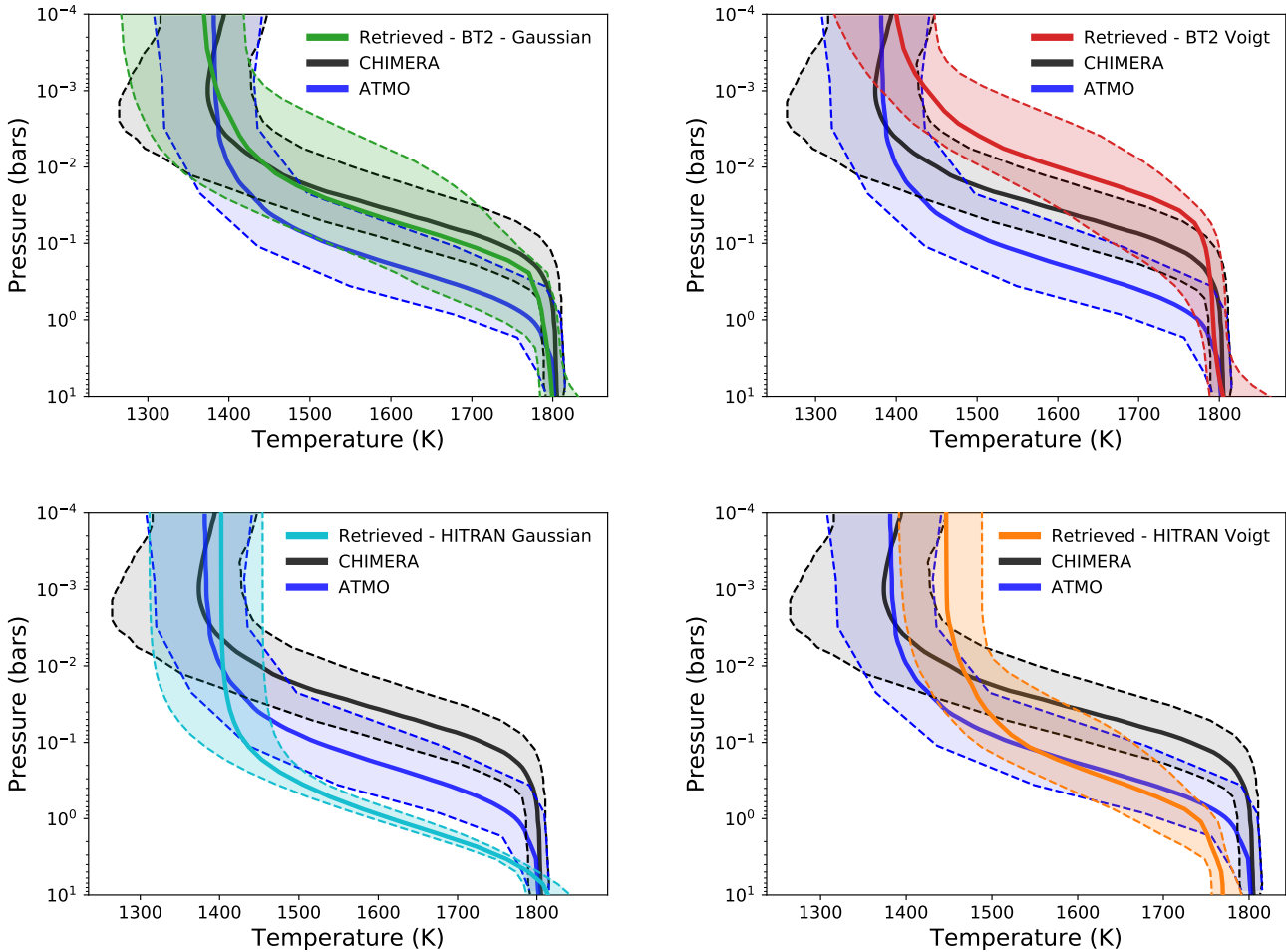


Figure 7. Comparison of the retrieved temperature profiles from real WASP-43b HST/WFC3 and Spitzer data from [Kreidberg et al. \(2014\)](#) using different H₂O line lists and line profile treatment (see text) compared to previous median retrieved temperature profiles (CHIMERA and ATMO from [Kreidberg et al. \(2014\)](#) and [Evans et al. \(2017\)](#), respectively). The colors for the PETRA retrievals match those in Figure 6.

in hot Jupiter atmospheres and considers many more transitions.

Each temperature profile in Figure 7 is qualitatively similar in shape and temperature range. There are some subtle differences, with the BT2 retrievals having a slightly different lapse rate than the BT2 retrieval with Voigt profiles. The HITRAN2008 retrieval with the Gaussian approximation exhibits a highly constrained lower atmosphere, uncharacteristic of the other profile. Additionally, the temperature profile was uniformly moved to lower pressures in the retrievals with Voigt line profiles compared to the same retrieval with Gaussian line profiles. This underestimation is because a Gaussian line profile will systematically underestimate the opacity for a given line, particularly the line wings. This means that the photosphere of the retrieved model will be deeper in the atmosphere when Gaussian line profiles are assumed. The BT2 retrieval with Gaus-

sian line profiles, however, matched very closely with the CHIMERA retrieval, though they used a HITEMP H₂O line list ([Rothman et al. 2010](#)), presumably with Voigt profiles. The HITEMP line list, an updated version of the HITRAN2008 list more appropriate for hot atmospheres like we consider here, uses the BT2 line list as its starting point.

The four different retrieved H₂O and CO₂ abundances are compared in Figure 9. Only the H₂O abundance is published in [Evans et al. \(2017\)](#). In general, all abundances agree quite well and are close to the solar abundance VMR of H₂O of about $10^{-3.6}$. The H₂O abundance found in the BT2 retrieval with Voigt profiles was slightly higher than the other retrievals. In general, there is a correlation between the pressure of the temperature profile (parameterized through κ_{IR} in [Line et al. \(2013\)](#)) and the molecular abundances. When the temperature profile is moved to lower pressures, the molecu-

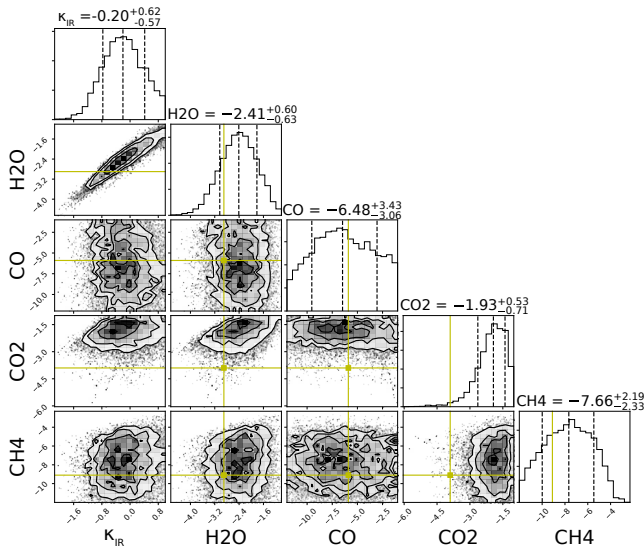


Figure 8. Posterior distribution for some parameters in the WASP-43b BT2 Voigt profile retrieval. Gold lines indicate the values found in Kreidberg et al. (2014).

lar abundances, particularly H_2O , must compensate by becoming larger to keep the same brightness temperature at a given wavelength. This correlation is shown in Figure 8, which displays the posteriors of the WASP-43b BT2 Voigt profile retrieval. The correlation between κ_{IR} and the chemical abundances likely explains some of the differences between the exact temperature profiles and abundances found in the ATMO, CHIMERA, and PETRA retrievals.

Three of the PETRA retrievals show a somewhat higher CO_2 abundance, but they agree at about the $1\text{-}\sigma$ level with the CHIMERA value, which used the HITEMP database (Rothman et al. 2010). The HITRAN2008 retrieval with Gaussian profiles showed a significantly lower CO_2 abundance, closer to the CHIMERA value. Additionally, note that most of the information for the CO_2 and CO abundances relies on the single *Spitzer* 4.5 micron point. PETRA and CHIMERA both seem to prefer fitting the *Spitzer* data with CO_2 rather than CO , however. Removing CO_2 does not change the goodness of fit, because CO can compensate; however, removing both CO and CO_2 changes the Bayesian Information Criterion (BIC) by about 20, indicating strong evidence for their inclusion in the model. The BIC quantifies whether the complexity of a given model is justified by the data by penalizing the likelihood by a factor proportional to the number of free-parameters (Schwarz 1978).

We also tested whether there was any evidence of a vertically non-uniform H_2O abundance by running a retrieval using the parameteri-

zation described in Section 2.1.2. While such a retrieval was able to constrain the H_2O abundance consistent with the uniform model, we find that the non-uniform model is not justified given the data, with a ΔBIC of 31.95 in favor of the simpler uniform abundance model. This is in agreement with the theoretical expectation that the H_2O abundance should be roughly uniform with pressure throughout much of the observable atmosphere in hot Jupiters in this temperature regime.

On the whole, assuming Gaussian line profiles can provide results qualitatively similar to Voigt line profiles. However because we do not expect thermal broadening to be the main source of line broadening in most exoplanet retrieval applications, assuming Voigt line profiles will provide the more physically accurate results. This exercise illustrates the model uncertainties present in retrieval analyses that emerge as a result of, e.g., line list choices. While we can assume that Voigt line profiles will provide a more realistic match to observations than Gaussian line profiles, some choices can be more arbitrary. When such cases arise, it is best to evaluate observations using a variety of model assumptions whenever possible, which can begin to quantify our systematic model uncertainties.

3.2.2. HD 209458b

In order to further compare PETRA with other retrieval suites, we retrieved the temperature profile and molecular abundances of hot Jupiter HD 209458b using HST/WFC3 and *Spitzer* data from Line et al. (2016). This same data was analyzed in Line et al. (2016) with the same CHIMERA retrieval suite as WASP-43b above and was found to show evidence for a non-inverted atmosphere with an approximately solar abundance of H_2O . For this retrieval, we use the BT2 line list with Voigt line profiles, which should most closely match the CHIMERA retrieval.

Our retrieval results agree quite well with the CHIMERA retrieval. Figure 10 shows the retrieved spectrum compared to the observations from Line et al. (2016). The median retrieved spectrum has $\chi^2 = 15.2$ with 14 data points, leading to a χ^2 per data point of 1.08. As with WASP-43b, PETRA fits the data as well as CHIMERA, which obtains a χ^2 per data point of 1.03.

Figure 11 shows that PETRA’s retrieved median temperature profile agrees quite well with CHIMERA’s, but is more tightly constrained than the CHIMERA profile using the same parameterization (that of Parmentier et al. (2013)). The PETRA profile is most similar to the CHIMERA retrieval using the simplified PT profile, which consists of a deep isothermal region and 2 “T linear-in-P” regions. This simplified CHIMERA profile

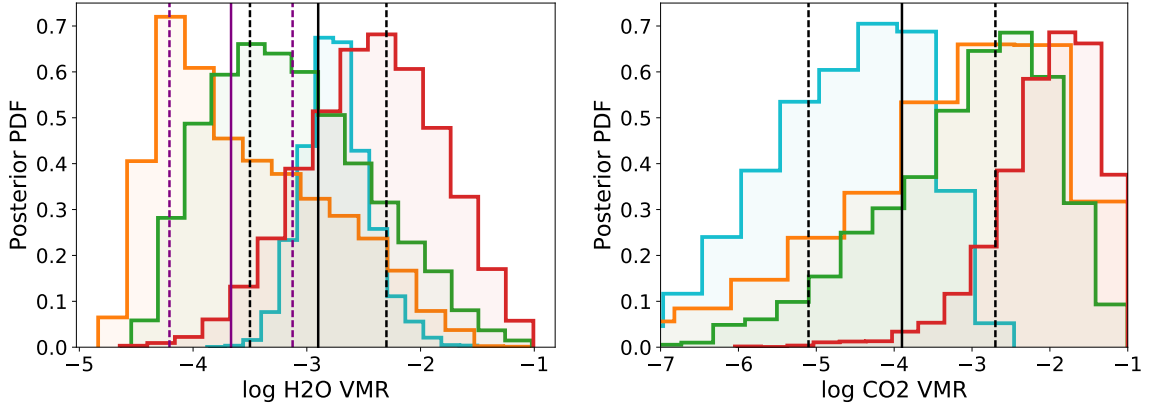


Figure 9. Posterior distributions of H_2O and CO_2 from real WASP-43b HST/WFC3 and *Spitzer* data from Kreidberg et al. (2014) using different H_2O line lists and/or molecular profiles, compared to previous retrieved (same colors and labels as Figures 6 and 7). Retrieved abundances and $1\text{-}\sigma$ from Kreidberg et al. (2014) are in black and from Evans et al. (2017) are in purple. Note that Evans et al. (2017) only presents the H_2O abundance.

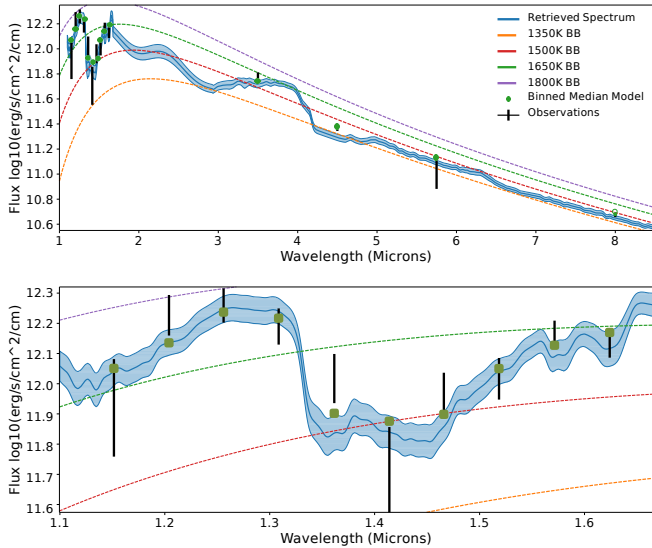


Figure 10. Retrieved planet spectrum with its $1\text{-}\sigma$ uncertainty region, convolved to the HST/WFC3 instrument resolution of $R\sim 130$, compared to observations of HD 209458b from Line et al. (2016). Green points represent the binned median retrieved spectrum. The bottom figure is a zoomed in version of the top, highlighting the 1.4 micron H_2O feature from HST/WFC3 observations.

also exhibits a more constrained profile compared to the CHIMERA retrieval with the 5-parameter Parmentier et al. (2013) parameterization. The CHIMERA retrieval also utilized nested sampling rather than DEMC, which may explain some of the differences with the PETRA retrieval.

Contribution function profiles are plotted in Figure 12, demonstrating that pressures between 5 and 100 mbar are constrained by the observations. As with WASP-43b, all constraints on the temperature profile outside

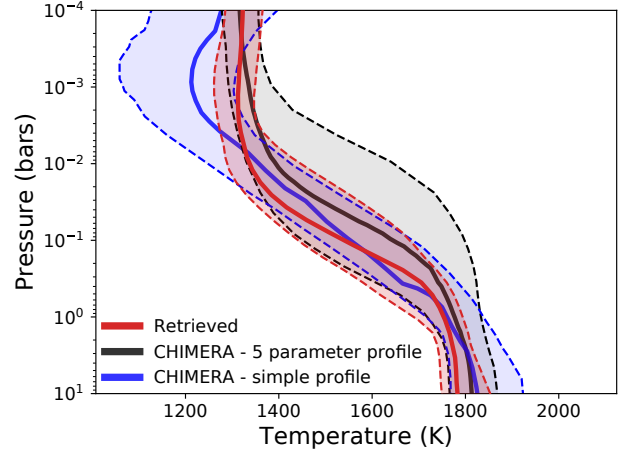


Figure 11. Retrieved temperature profile of the HD 209458b data compared with the median retrieved temperature profile from (Line et al. 2016). Our median retrieved temperature profile agrees with those from the CHIMERA retrieval suite, though our $1\text{-}\sigma$ range is much tighter. This may be because of differences in line lists and statistical framework.

this range are a consequence of the parameterization of the temperature profile.

Figure 13 shows that the molecular abundance constraints PETRA retrieves are also well within $2\text{-}\sigma$ of CHIMERA's retrieved constraints, despite the different statistical framework and different line lists being used between the two suites. Line et al. (2016) uses HITEMP H_2O , CO , and CO_2 (Rothman et al. 2010), while we use CO_2 from (Rothman et al. 2009), CO from Goorvitch (1994), and H_2O from Barber et al. (2006).

The inclusion of H_2O is strongly favored with change in the BIC of 35. When we neglected CO and CO_2 ,

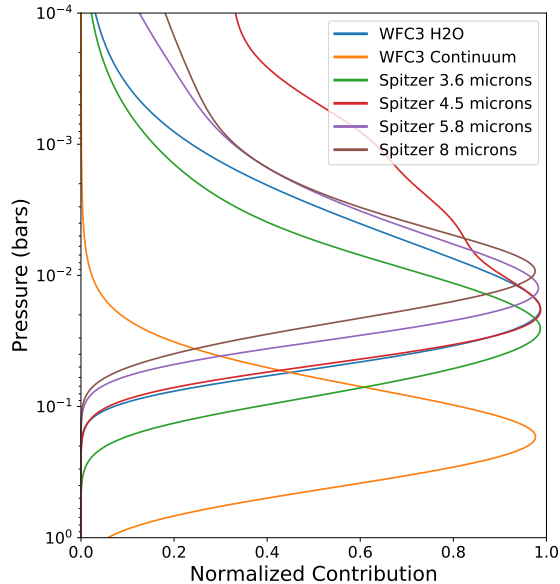


Figure 12. Contribution functions for HD 209458b’s dayside atmosphere at 1.25, 1.4, 3.6, and 4.5 μm , corresponding to outside the 1.4 μm H_2O feature, inside the 1.4 μm H_2O feature, and channel 1, 2, 3, and 4 from *Spitzer*, respectively.

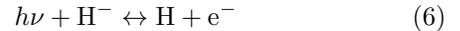
PETRA attempted to compensate by increasing the HCN abundance to a $\log_{10}(\text{VMR}) = 2.7$. Because HCN also absorbs 1.53 μm , this also resulted in the H_2O abundance decreasing by about an order of magnitude. When CO, CO_2 , and HCN are all ignored, we calculate a BIC of 5.06, indicating positive evidence for absorption by a carbon species in the atmosphere of HD209458b, in agreement with [Line et al. \(2016\)](#).

4. CHARACTERIZING ULTRA-HOT JUPITERS WITH RETRIEVALS OF H^-

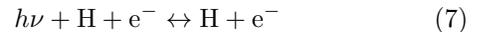
Ultra-hot Jupiters are among the most ideal targets to observe because of their hot, bright daysides, their inflated radii, and their short periods. However, ultra-hot Jupiter atmospheres are often hot enough to dissociate the very molecules we hope to observe. The absence of molecules is exacerbated by the fact that H^- bound-free and free-free opacity becomes significant at temperatures above 2500 K, which will move the photosphere to lower pressures and mask the spectral features of molecules like H_2O ([Arcangeli et al. 2018](#); [Parmentier et al. 2018](#); [Lothringer et al. 2018](#); [Kitzmann et al. 2018](#)). This phenomenon is thought to explain the absence of H_2O in WASP-12b, WASP-18b, WASP-103, and HAT-P-7b ([Arcangeli et al. 2018](#); [Kreidberg et al. 2018](#); [Mansfield et al. 2018](#)).

In order to characterize the atmospheres of ultra-hot Jupiters, we must look to non-molecular spectral sig-

natures. While H^- opacity mutes molecular spectral features, it also has the potential to help characterize ultra-hot Jupiter atmospheres. H^- opacity is dominant at the temperatures and pressures in ultra-hot Jupiters and, importantly, is non-grey, which means that we can use H^- to probe different pressures in ultra-hot Jupiters. In fact, H^- opacity increases steadily with increasing wavelength from its minimum at about 1.6 μm because of its free-free interactions:



([Wildt 1939](#)). Similarly, H^- opacity increases towards short wavelengths from the minimum at 1.6 μm until 0.85 μm because of its bound-free interaction



([Pannekoek 1931](#)). Fortunately, this near-IR wavelength range will be explored to great precision with JWST.

Taken a step further, we can use H^- to constrain the e^- density. H^- opacity will scale with the product of the e^- and H densities in LTE:

$$\alpha_{\text{H}^-} = n_{\text{H}}n_{e^-}\sigma_{\text{H}^-} \quad (8)$$

where α_{H^-} is the absorption coefficient for H^- , n_{H} is the number density of atomic H, n_{e^-} is the e^- number density, and σ_{H^-} is the cross-section for H^- in cm^2 from [John \(1988\)](#). n_{H} will remain relatively constant with height at pressures above 1 μbar , so we chose to use its equilibrium abundance rather than allow it to be a free parameter. Note that neither Equation 7 nor 8 contain the actual abundance of H^- , as it is ill-defined in the free-free interaction

4.1. KELT-9b

KELT-9b is the hottest known Jovian planet with a dayside-redistribution equilibrium temperature of about 4500 K ([Gaudi et al. 2017](#)), over 1000 K hotter than the next hottest Jovian planet, WASP-33b². KELT-9b provides an ideal example to explore ultra-hot Jupiter characterization through H^- . In a planet like KELT-9b, the brightness temperature observed in secondary eclipse can vary by nearly 1000 K between 2 and 10 μm due to H^- opacity (see Figure 14 and see Figure 15 in [Lothringer et al. 2018](#)). This corresponds to probing about an order of magnitude in pressure between 10 and 100 mbar, useful for determining the presence and magnitude of temperature inversions which are predicted to be ubiquitous in the hottest Jovian planets ([Lothringer](#)

² <https://exo.mast.stsci.edu/>

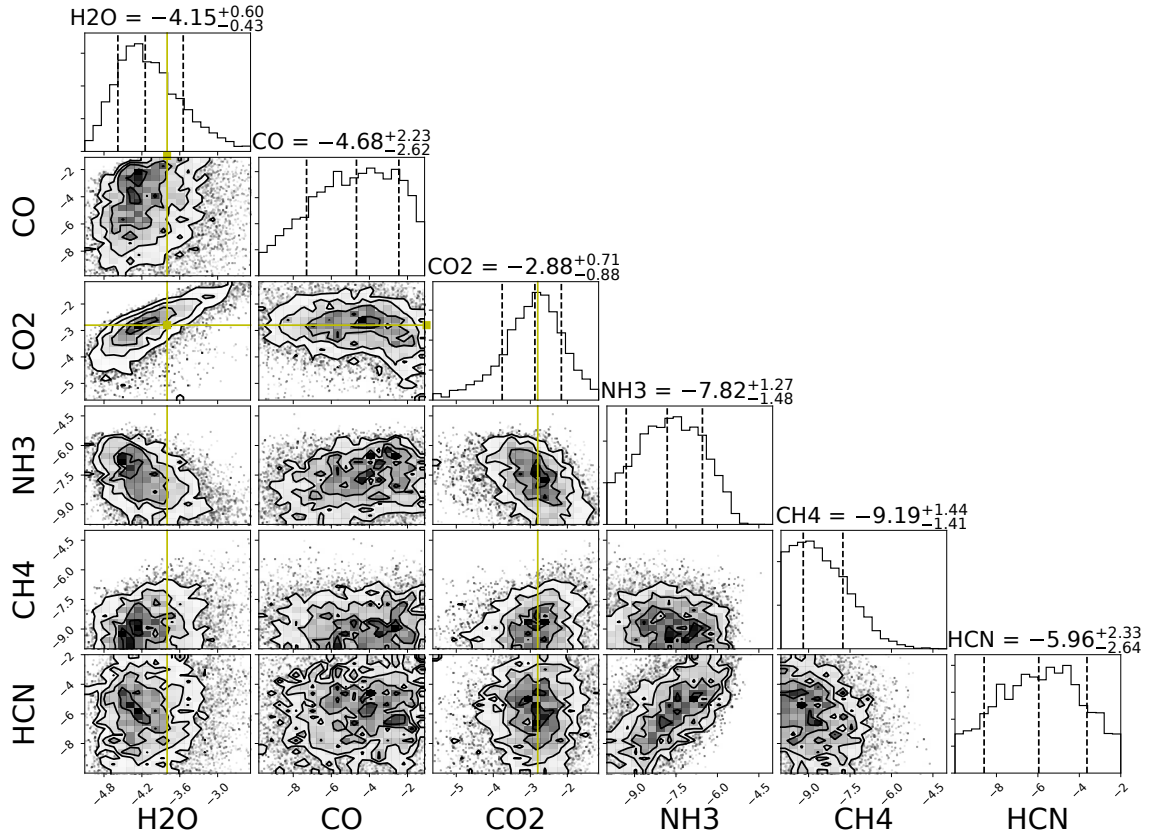


Figure 13. Posterior distributions for the molecular abundances from PETRA’s retrieval of HD 209458b (Line et al. 2016). Gold lines represent the approximate maximum of the posterior from (Line et al. 2016) for the two species with obvious maxima, H₂O and CO₂.

et al. 2018). Indeed, a temperature inversion has recently been detected in KELT-9b from ground-based high-resolution observations of neutral Fe (Pino et al. 2020).

4.1.1. Retrieval with PETRA

In order to explore the possibility of retrieving atmospheric properties from ultra-hot Jupiters using H⁻ opacity, we simulate a single secondary eclipse of KELT-9b with both JWST/NIRSPEC/G235H and G395H with PandExo (Batalha et al. 2017). We input to PandExo a fully self-consistent model of KELT-9b, assuming dayside-heat redistribution, from (Lothringer et al. 2018). The use of a self-consistent model helps to test the retrieval forward model parameterizations and assumptions described below.

The G235H and G395H grisms span 1.67-5.14 μm at resolutions of about $R \sim 2,700$ with some overlap between 2.87 and 3.05 μm . Shorter wavelength and lower resolution observations are made difficult because of saturation from KELT-9b’s bright A0 host star ($V=7.6$). The broad wavelength coverage afforded by JWST is essential to maximizing brightness temperature contrasts since H⁻ opacity increases steadily but slowly

across the wavelength range. Figure 14 shows the simulated observations with blackbodies over-plotted for reference, demonstrating that the brightness temperature of KELT-9b changes by over 300 K in the G235H and G395H wavelength region. The contribution functions plotted in Figure 15 show that about an order of magnitude in pressure between 10 and 100 mbar is probed between 1.6 and 5 μm .

We then used PETRA to retrieve atmospheric properties from the simulated KELT-9b observations. We chose to retrieve the temperature structure, the CO abundance, and the e⁻ density using H⁻ opacity as a proxy, while holding other abundances to their chemical equilibrium value. Besides H⁻, our models suggest CO is the only opacity source detectable at low-resolution.

Molecular, atomic, and ion abundances will likely not be uniform with altitude in KELT-9b’s atmosphere due to thermal and photo-ionization, as well as the thermal dissociation of molecules. It is therefore necessary to parameterize retrieved chemical abundances. We ran three different scenarios where **1**) CO is assumed to be in chemical equilibrium, **2**) the CO abundance is retrieved assuming a vertically-uniform abundance, and

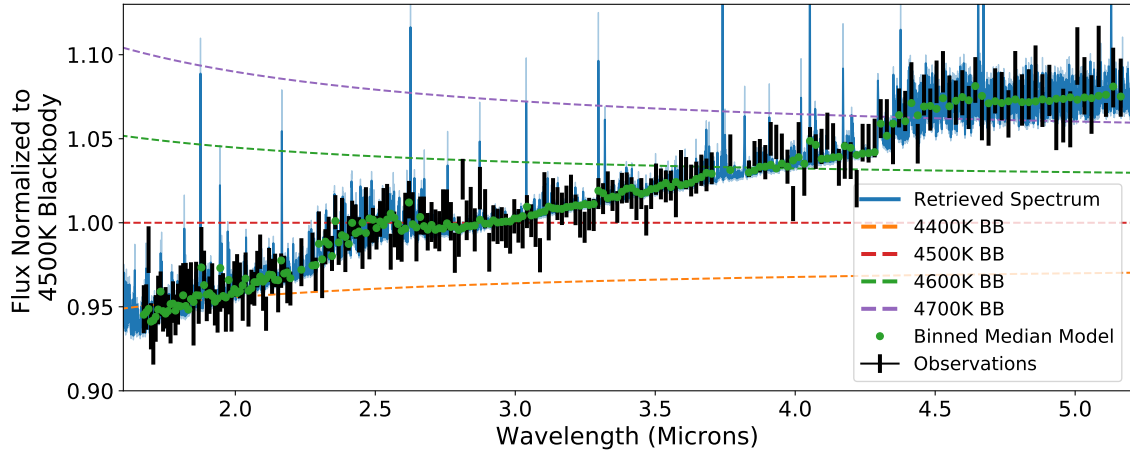


Figure 14. Retrieved median spectrum (blue) for the retrieval where CO is assumed to be in chemical abundance, normalized by a 4500 K blackbody and compared to the simulated observations for the KELT-9b retrieval (black). The 1- σ uncertainty region is shaded, but small compared to the individual error bars. The green dots represent the binned flux of the median retrieved model.

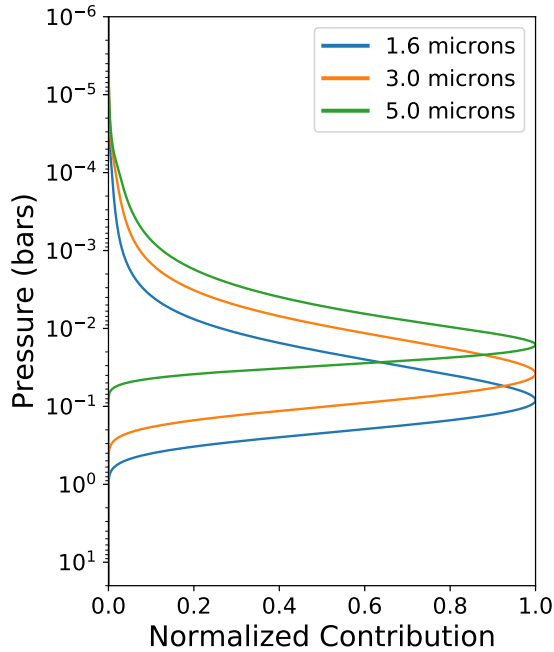


Figure 15. Contribution functions for KELT-9's dayside atmosphere at 1.6, 3.0, and 5.0 μm from the median retrieved model.

3) the CO abundance is retrieved using the evidence of a vertically non-uniform H₂O abundance parameterization described in Section 2.1.2. For each of these scenarios, the e^- abundance is also retrieved, assuming a non-uniform abundance.

Figure 14 shows the retrieved median spectrum for the retrieval where CO is assumed to be in chemical equilibrium with the 1- σ uncertainty region compared to the simulated observations. The uncertainties on the

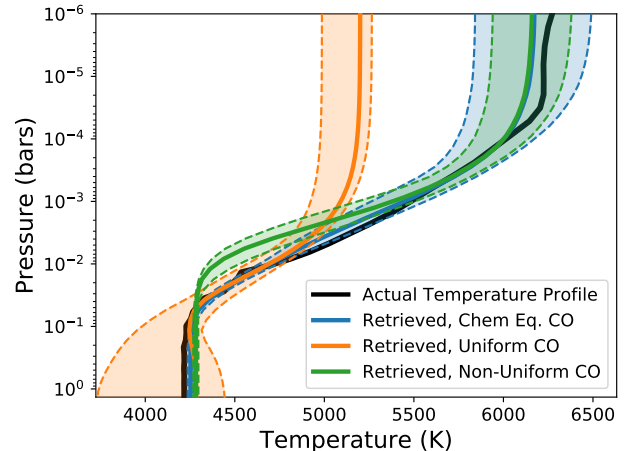


Figure 16. Simulated constraints on the temperature structure of KELT-9b for the three retrieval scenarios, where CO is assumed to be in chemical equilibrium, have a vertically-uniform abundance, or a parameterized evidence of a vertically non-uniform H₂O abundance.

flux for a given wavelength point are much smaller than an individual bin's observational uncertainty.

Figure 16 and 17 shows the retrieved constraints on the temperature structure and chemical abundances (in the form of volume mixing ratio), respectively, for each retrieval. The temperature structure is tightly constrained by the retrieval, clearly identifying the strong temperature inversion, however accurate temperatures are only retrieved near the photosphere. Further, the retrieval where CO is parameterized as having a non-uniform abundance (i.e., the model with the most free

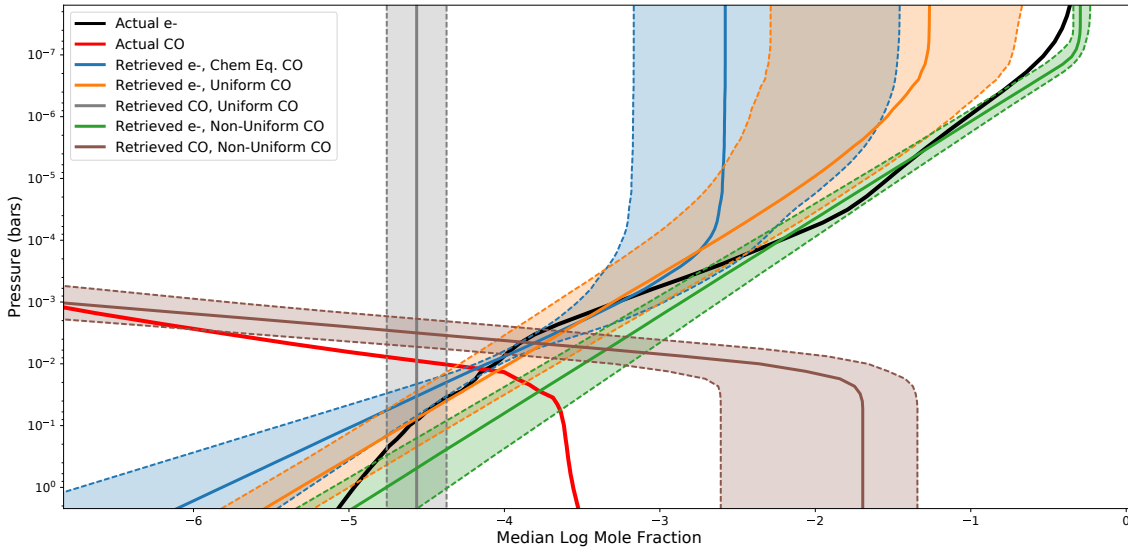


Figure 17. Simulated constraints on the abundances of e^- and CO for the three KELT-9b retrieval scenarios, where CO is assumed to be in chemical equilibrium, have a vertically-uniform abundance, or a parameterized evidence of a vertically non-uniform H₂O abundance abundance.

parameters), actually has the least accurate fit and is biased towards a lower-pressure photosphere.

Figure 17 shows the retrieved chemical abundances compared to the actual abundances of e^- and CO in the input model. When CO is assumed to be in chemical equilibrium, accurate constraints on the e^- density can be obtained. Similarly, if CO is assumed to have a vertically-uniform abundance, accurate e^- and CO abundances are retrieved, albeit with the foreknowledge that the uniform CO abundance can only be an approximation. Interestingly, however, when both CO and e^- are retrieved using the non-uniform parameterization, the abundances are biased to higher values, which help place the photosphere at a lower pressure as described above.

The reason for the behavior seen when CO and e^- are retrieved non-uniformly is due to the fact that there is a degeneracy between the photospheric level and the chemical abundances. In the [Parmentier & Guillot \(2014\)](#) temperature structure parameterization, the pressure-level of the photosphere is controlled through the κ_{IR} parameter which physically represents the mean opacity of the IR and sets the relation between the optical depth and pressure. Figure 18 shows the posterior distribution for the chemical abundance parameters and the κ_{IR} parameter. A clear correlation exists between κ_{IR} and the e^- abundance parameters. There is also some degeneracy between the slope of the e^- density, η_{0,e^-} , and the CO abundance parameters.

A degeneracy between the abundance parameters and κ_{IR} exists because there is no non-retrieved opacity that can set the photospheric level. In the case where CO is

assumed to be in chemical equilibrium, the relation between the brightness temperature at 2.3 and 4.5 microns and the CO opacity at those wavelengths effectively anchors the temperature structure. Indeed, the degeneracy is broken in the retrieval where CO is in chemical equilibrium and can be used as such an anchor.

This situation is similar to the well-known degeneracy in transit spectra between the reference radius and pressure ([Griffith 2014](#); [Heng & Kitzmann 2017](#)). This degeneracy can be broken through information about the scale height from the Rayleigh scattering slope ([Benneke & Seager 2012](#); [Line & Parmentier 2016](#)) or from the continuum level from H₂ CIA opacity ([Welbanks & Madhusudhan 2019](#)). H⁻ opacity would serve to similarly break the degeneracy in for ultra-hot Jupiters. In our retrieved emission spectrum, however, we retrieved both the continuum opacity and the CO abundance and had nothing to anchor the photospheric level of the atmosphere. An assumption, like chemical equilibrium of CO, provides this anchor and breaks the correlation.

The power of H⁻ retrievals lies not only in their ability to constrain ultra-hot Jupiter temperature structures, but also in the retrieval’s measurement of n_{e^-} . A deviation in n_{e^-} from chemical equilibrium could identify and measure the effects of photoionization in these highly irradiated atmospheres. Additionally, a direct measurement of the ion density will provide a path forward to understanding magneto-hydrodynamic (MHD) effects in ultra-hot Jupiters, which are likely affecting atmospheric circulation through magnetic drag forces ([Rogers & Komacek 2014](#); [Komacek & Showman 2016](#); [Rogers & McElwaine 2017](#)). The combination of ion density mea-

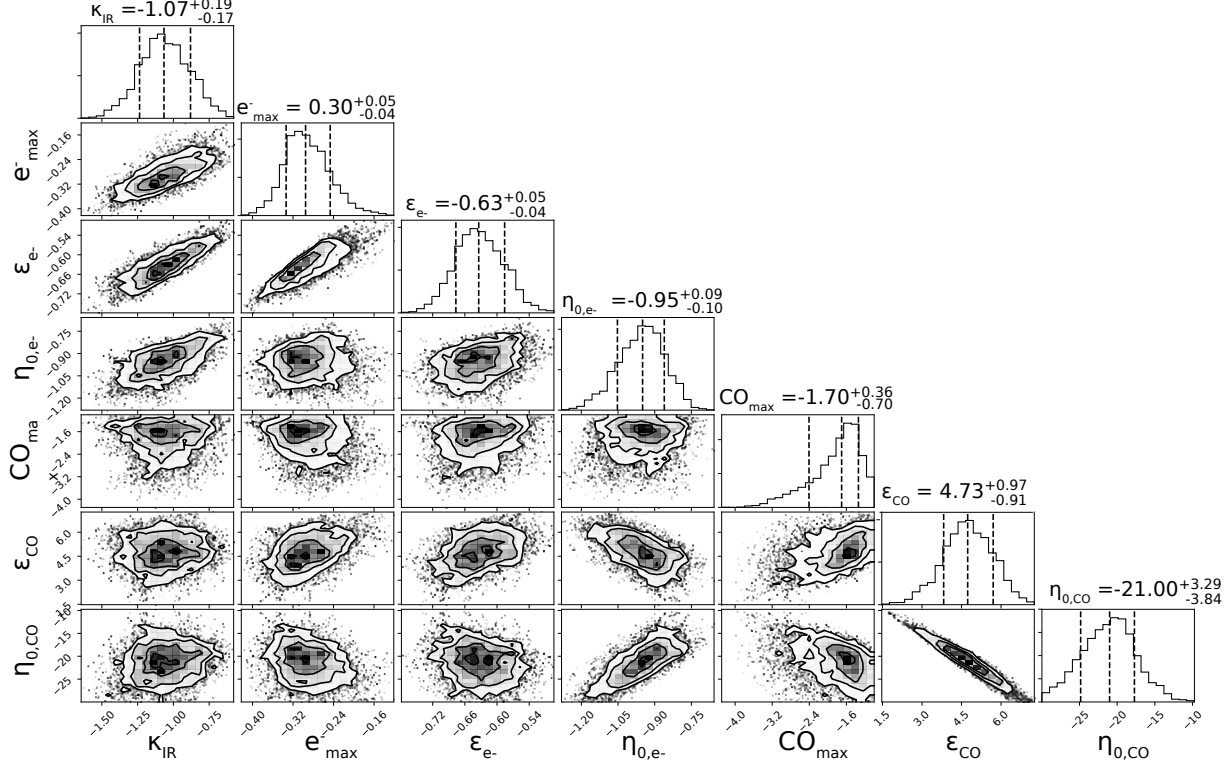


Figure 18. Posterior distributions for the KELT-9b retrieval where a evidence of a vertically non-uniform H₂O abundance CO abundance parameterization was used. For clarity, most temperature structure parameters were not included. Note the correlations between κ_{IR} , e_{max} , and η_{0,e^-} , as well as the correlations between η_{0,e^-} , $\eta_{0,CO}$, and ϵ_{CO} .

measurements through H⁻ retrievals along with wind speed measurements from high-dispersion spectroscopy (Brogi et al. 2016, e.g.,) and day-night temperature contrasts from phase curves will provide direct insight into MHD effects.

We also note that rather than using H⁻ as a free variable, it can be used in retrievals of metallicity that assume chemical equilibrium (Arcangeli et al. 2018). When used in this fashion, H⁻ can help constrain the metallicity because it will depend on the number of free electrons, which will be supplied from metals like Na, K, and Ca. This would not account for the effect of photoionization, however.

5. CONCLUSION

We have introduced the PHOENIX Exoplanet Retrieval Algorithm, or PETRA, which is a retrieval framework built around the PHOENIX atmosphere model. PETRA is flexible enough to retrieve atmospheric properties from observations of exoplanets, brown dwarfs, and even stars for a variety of situations, including transit and eclipse spectroscopy, as well as self-luminous/directly-imaged objects.

We have validated PETRA by retrieving properties from data simulated from PHOENIX models, for which

the correct atmospheric properties are known. PETRA is successfully able to retrieve these correct properties. We have further validated PETRA against previous retrieval results for actual HST/WFC3 and *Spitzer* observations of WASP-43b and HD 209458b, showing that PETRA can agree with well-tested retrievals like CHIMERA and ATMO. For WASP-43b, we also investigated the effect that different H₂O line lists and line shape treatments have on retrieved quantities, showing significant differences especially in the retrieved temperature profiles. Our results are similar to those of (Barstow et al. 2020), which demonstrated comparable agreement between retrieval suites and the importance of line broadening treatment.

We then used PETRA to demonstrate a novel technique to characterize ultra-hot Jupiters through retrieving H⁻. Retrievals using current techniques (i.e., retrieving molecular abundances) are hampered by the thermal dissociation of molecules and presence of H⁻ opacity at high temperatures. Using simulated JWST/NIRSPEC data, we showed that retrieving the H⁻ can constrain the temperature structure and e⁻ density, providing a unique path forward towards characterizing the hottest Jovian exoplanets. We discovered that an assumption about the CO opacity is critical to using

H^- in a retrieval due to correlations between the parameters that set the photospheric level of the temperature structure and the chemical abundances. We note that ground-based high-resolution studies will be insensitive to the continuous opacity of H^- , meaning that JWST may be the only facility capable of this experiment until the *ARIEL* mission (Pascale et al. 2018).

PETRA will be continually improved. We plan to incorporate PHOENIX’s cloud modeling capabilities into PETRA to perform retrievals of cool objects. We will also improve the statistical framework by implementing nested sampling in order to robustly perform model complexity comparison. In the future, we will apply PETRA to a variety of situations, from transmission spectra of sub-Neptunes to high resolution spectroscopy of giant planets.

ACKNOWLEDGMENTS

We thank the anonymous referee for helpful comments that improved the manuscript. We also thank Ian Crossfield, Tommi Koskinen, Roger Yelle, and Andrew Youdin for constructive feedback and discussion. This research has made use of the NASA Astrophysics Data System and the NASA Exoplanet Archive, which is operated by the California Institute of Technology, under contract with the National Aeronautics and Space Administration under the Exoplanet Exploration Program. Allocation of computer time from the UA Research Computing High Performance Computing (HPC) at the University of Arizona is also gratefully acknowledged.

Software: Corner (Foreman-Mackey 2016), PandExo (Batalha et al. 2017), Astropy (Astropy Collaboration et al. 2013)

REFERENCES

- Allard, F., Homeier, D., & Freytag, B. 2011, in *Astronomical Society of the Pacific Conference Series*, Vol. 448, 16th Cambridge Workshop on Cool Stars, Stellar Systems, and the Sun, ed. C. Johns-Krull, M. K. Browning, & A. A. West, 91.
<https://arxiv.org/abs/1011.5405>
- Arcangeli, J., Désert, J.-M., Line, M. R., et al. 2018, *ApJL*, 855, L30, doi: [10.3847/2041-8213/aab272](https://doi.org/10.3847/2041-8213/aab272)
- Astropy Collaboration, Robitaille, T. P., Tollerud, E. J., et al. 2013, *A&A*, 558, A33, doi: [10.1051/0004-6361/201322068](https://doi.org/10.1051/0004-6361/201322068)
- Barber, R. J., Tennyson, J., Harris, G. J., & Tolchenov, R. N. 2006, *MNRAS*, 368, 1087, doi: [10.1111/j.1365-2966.2006.10184.x](https://doi.org/10.1111/j.1365-2966.2006.10184.x)
- Barman, T. S., Hauschildt, P. H., & Allard, F. 2001, *ApJ*, 556, 885, doi: [10.1086/321610](https://doi.org/10.1086/321610)
- Barman, T. S., Macintosh, B., Konopacky, Q. M., & Marois, C. 2011, *ApJ*, 733, 65, doi: [10.1088/0004-637X/733/1/65](https://doi.org/10.1088/0004-637X/733/1/65)
- Barstow, J. K., Aigrain, S., Irwin, P. G. J., & Sing, D. K. 2017, *ApJ*, 834, 50, doi: [10.3847/1538-4357/834/1/50](https://doi.org/10.3847/1538-4357/834/1/50)
- Barstow, J. K., Changeat, Q., Garland, R., et al. 2020, *MNRAS*, 493, 4884, doi: [10.1093/mnras/staa548](https://doi.org/10.1093/mnras/staa548)
- Barstow, J. K., & Heng, K. 2020, arXiv e-prints, arXiv:2003.14311. <https://arxiv.org/abs/2003.14311>
- Batalha, N. E., Mandell, A., Pontoppidan, K., et al. 2017, *PASP*, 129, 064501, doi: [10.1088/1538-3873/aa65b0](https://doi.org/10.1088/1538-3873/aa65b0)
- Benneke, B., & Seager, S. 2012, *ApJ*, 753, 100, doi: [10.1088/0004-637X/753/2/100](https://doi.org/10.1088/0004-637X/753/2/100)
- Brogi, M., de Kok, R. J., Albrecht, S., et al. 2016, *ApJ*, 817, 106, doi: [10.3847/0004-637X/817/2/106](https://doi.org/10.3847/0004-637X/817/2/106)
- Brogi, M., Line, M., Bean, J., Désert, J.-M., & Schwarz, H. 2017, *ApJL*, 839, L2, doi: [10.3847/2041-8213/aa6933](https://doi.org/10.3847/2041-8213/aa6933)
- Brogi, M., Line, M. R., Brogi, M., & Line, M. R. 2019, *AJ*, 157, 114, doi: [10.3847/1538-3881/aaffd3](https://doi.org/10.3847/1538-3881/aaffd3)
- Burningham, B., Marley, M. S., Line, M. R., et al. 2017, *MNRAS*, 470, 1177, doi: [10.1093/mnras/stx1246](https://doi.org/10.1093/mnras/stx1246)
- Evans, T. M., Sing, D. K., Kataria, T., et al. 2017, *Nature*, 548, 58, doi: [10.1038/nature23266](https://doi.org/10.1038/nature23266)
- Fisher, C., Hoeijmakers, H. J., Kitzmann, D., et al. 2019, arXiv e-prints, arXiv:1910.11627. <https://arxiv.org/abs/1910.11627>
- Foreman-Mackey, D. 2016, *The Journal of Open Source Software*, 1, 24, doi: [10.21105/joss.00024](https://doi.org/10.21105/joss.00024)
- Gandhi, S., & Madhusudhan, N. 2018, *MNRAS*, 474, 271, doi: [10.1093/mnras/stx2748](https://doi.org/10.1093/mnras/stx2748)
- Gandhi, S., Madhusudhan, N., Hawker, G., & Piette, A. 2019, arXiv e-prints, arXiv:1910.14042. <https://arxiv.org/abs/1910.14042>
- Gaudi, B. S., Stassun, K. G., Collins, K. A., et al. 2017, *Nature*, 546, 514, doi: [10.1038/nature22392](https://doi.org/10.1038/nature22392)
- Gelman, A., & Rubin, D. B. 1992, *Statistical Science*, 7, 457, doi: [10.1214/ss/1177011136](https://doi.org/10.1214/ss/1177011136)

- Gibson, N. P., Merritt, S., Nugroho, S. K., et al. 2020, arXiv e-prints, arXiv:2001.06430.
<https://arxiv.org/abs/2001.06430>
- Goorvitch, D. 1994, *ApJS*, 95, 535, doi: [10.1086/192110](https://doi.org/10.1086/192110)
- Gottwald, M., & Bovensmann, H. 2011, *SCIAMACHY - Exploring the Changing Earth's Atmosphere*, 1, doi: [10.1007/978-90-481-9896-2](https://doi.org/10.1007/978-90-481-9896-2)
- Gravity Collaboration, Nowak, M., Lacour, S., et al. 2020, *A&A*, 633, A110, doi: [10.1051/0004-6361/201936898](https://doi.org/10.1051/0004-6361/201936898)
- Gray, D. F. 1992, *The observation and analysis of stellar photospheres.*, Vol. 20 (Cambridge University Press, Cambridge, UK)
- Griffith, C. A. 2014, *Philosophical Transactions of the Royal Society of London Series A*, 372, 20130086, doi: [10.1098/rsta.2013.0086](https://doi.org/10.1098/rsta.2013.0086)
- Hauschildt, P. H., Allard, F., & Baron, E. 1999, *ApJ*, 512, 377, doi: [10.1086/306745](https://doi.org/10.1086/306745)
- Hauschildt, P. H., Baron, E., & Allard, F. 1997, *ApJ*, 483, 390, doi: [10.1086/304233](https://doi.org/10.1086/304233)
- Heng, K., & Kitzmann, D. 2017, *MNRAS*, 470, 2972, doi: [10.1093/mnras/stx1453](https://doi.org/10.1093/mnras/stx1453)
- Himes, M. D., Harrington, J., Cobb, A. D., et al. 2020, arXiv e-prints, arXiv:2003.02430.
<https://arxiv.org/abs/2003.02430>
- Hjerting, F. 1938, *ApJ*, 88, 508, doi: [10.1086/144000](https://doi.org/10.1086/144000)
- Howe, A. R., Burrows, A., & Deming, D. 2017, *ApJ*, 835, 96, doi: [10.3847/1538-4357/835/1/96](https://doi.org/10.3847/1538-4357/835/1/96)
- Irwin, P. G. J., Teanby, N. A., de Kok, R., et al. 2008, *JQSRT*, 109, 1136, doi: [10.1016/j.jqsrt.2007.11.006](https://doi.org/10.1016/j.jqsrt.2007.11.006)
- John, T. L. 1988, *A&A*, 193, 189
- Kitzmann, D., Heng, K., Oreshenko, M., et al. 2020, *ApJ*, 890, 174, doi: [10.3847/1538-4357/ab6d71](https://doi.org/10.3847/1538-4357/ab6d71)
- Kitzmann, D., Heng, K., Rimmer, P. B., et al. 2018, *ApJ*, 863, 183, doi: [10.3847/1538-4357/aace5a](https://doi.org/10.3847/1538-4357/aace5a)
- Komacek, T. D., & Showman, A. P. 2016, *ApJ*, 821, 16, doi: [10.3847/0004-637X/821/1/16](https://doi.org/10.3847/0004-637X/821/1/16)
- Kreidberg, L., Bean, J. L., Désert, J.-M., et al. 2014, *ApJL*, 793, L27, doi: [10.1088/2041-8205/793/2/L27](https://doi.org/10.1088/2041-8205/793/2/L27)
- Kreidberg, L., Line, M. R., Bean, J. L., et al. 2015, *ApJ*, 814, 66, doi: [10.1088/0004-637X/814/1/66](https://doi.org/10.1088/0004-637X/814/1/66)
- Kreidberg, L., Line, M. R., Parmentier, V., et al. 2018, *AJ*, 156, 17, doi: [10.3847/1538-3881/aac3df](https://doi.org/10.3847/1538-3881/aac3df)
- Lavie, B., Ehrenreich, D., Bourrier, V., et al. 2017, *A&A*, 605, L7, doi: [10.1051/0004-6361/201731340](https://doi.org/10.1051/0004-6361/201731340)
- Lee, J.-M., Heng, K., & Irwin, P. G. J. 2013, *ApJ*, 778, 97, doi: [10.1088/0004-637X/778/2/97](https://doi.org/10.1088/0004-637X/778/2/97)
- Line, M. R., Fortney, J. J., Marley, M. S., & Sorahana, S. 2014a, *ApJ*, 793, 33, doi: [10.1088/0004-637X/793/1/33](https://doi.org/10.1088/0004-637X/793/1/33)
- Line, M. R., Knutson, H., Wolf, A. S., & Yung, Y. L. 2014b, *ApJ*, 783, 70, doi: [10.1088/0004-637X/783/2/70](https://doi.org/10.1088/0004-637X/783/2/70)
- Line, M. R., & Parmentier, V. 2016, *Astrophys. J.*, 820, 78, doi: [10.3847/0004-637X/820/1/78](https://doi.org/10.3847/0004-637X/820/1/78)
- Line, M. R., Teske, J., Burningham, B., Fortney, J. J., & Marley, M. S. 2015, *ApJ*, 807, 183, doi: [10.1088/0004-637X/807/2/183](https://doi.org/10.1088/0004-637X/807/2/183)
- Line, M. R., Zhang, X., Vasisht, G., et al. 2012, *ApJ*, 749, 93, doi: [10.1088/0004-637X/749/1/93](https://doi.org/10.1088/0004-637X/749/1/93)
- Line, M. R., Wolf, A. S., Zhang, X., et al. 2013, *ApJ*, 775, 137, doi: [10.1088/0004-637X/775/2/137](https://doi.org/10.1088/0004-637X/775/2/137)
- Line, M. R., Stevenson, K. B., Bean, J., et al. 2016, *AJ*, 152, 203, doi: [10.3847/0004-6256/152/6/203](https://doi.org/10.3847/0004-6256/152/6/203)
- Line, M. R., Marley, M. S., Liu, M. C., et al. 2017, *ApJ*, 848, 83, doi: [10.3847/1538-4357/aa7ff0](https://doi.org/10.3847/1538-4357/aa7ff0)
- Lothringer, J. D., & Barman, T. 2019, *ApJ*, 876, 69, doi: [10.3847/1538-4357/ab1485](https://doi.org/10.3847/1538-4357/ab1485)
- Lothringer, J. D., Barman, T., & Koskinen, T. 2018, *ApJ*, 866, 27, doi: [10.3847/1538-4357/aadd9e](https://doi.org/10.3847/1538-4357/aadd9e)
- MacDonald, R. J., & Madhusudhan, N. 2017, *MNRAS*, 469, 1979, doi: [10.1093/mnras/stx804](https://doi.org/10.1093/mnras/stx804)
- Madhusudhan, N. 2018, *Atmospheric Retrieval of Exoplanets (Handbook of Exoplanets)*, 104, doi: [10.1007/978-3-319-55333-7_104](https://doi.org/10.1007/978-3-319-55333-7_104)
- Madhusudhan, N., & Seager, S. 2009, *ApJ*, 707, 24, doi: [10.1088/0004-637X/707/1/24](https://doi.org/10.1088/0004-637X/707/1/24)
- Mansfield, M., Bean, J. L., Line, M. R., et al. 2018, *AJ*, 156, 10, doi: [10.3847/1538-3881/aac497](https://doi.org/10.3847/1538-3881/aac497)
- McKemmish, L. K., Masseron, T., Hoesijmakers, H. J., et al. 2019, arXiv e-prints, arXiv:1905.04587.
<https://arxiv.org/abs/1905.04587>
- Mollière, P., Wardenier, J. P., van Boekel, R., et al. 2019, *A&A*, 627, A67, doi: [10.1051/0004-6361/201935470](https://doi.org/10.1051/0004-6361/201935470)
- Pannekoek, A. 1931, *MNRAS*, 91, 519, doi: [10.1093/mnras/91.5.519](https://doi.org/10.1093/mnras/91.5.519)
- Parmentier, V., & Guillot, T. 2014, *A&A*, 562, A133, doi: [10.1051/0004-6361/201322342](https://doi.org/10.1051/0004-6361/201322342)
- Parmentier, V., Showman, A. P., & Lian, Y. 2013, *A&A*, 558, A91, doi: [10.1051/0004-6361/201321132](https://doi.org/10.1051/0004-6361/201321132)
- Parmentier, V., Line, M. R., Bean, J. L., et al. 2018, *A&A*, 617, A110, doi: [10.1051/0004-6361/201833059](https://doi.org/10.1051/0004-6361/201833059)
- Pascale, E., Bezawada, N., Barstow, J., et al. 2018, in *Society of Photo-Optical Instrumentation Engineers (SPIE) Conference Series*, Vol. 10698, Proc. SPIE, 106980H, doi: [10.1117/12.2311838](https://doi.org/10.1117/12.2311838)
- Patrascu, A. T., Yurchenko, S. N., & Tennyson, J. 2015, *MNRAS*, 449, 3613, doi: [10.1093/mnras/stv507](https://doi.org/10.1093/mnras/stv507)
- Pino, L., Désert, J. M., Brogi, M., et al. 2020, arXiv e-prints, arXiv:2004.11335.
<https://arxiv.org/abs/2004.11335>
- Rogers, T. M., & Komacek, T. D. 2014, *ApJ*, 794, 132, doi: [10.1088/0004-637X/794/2/132](https://doi.org/10.1088/0004-637X/794/2/132)

- Rogers, T. M., & McElwaine, J. N. 2017, *ApJL*, 841, L26, doi: [10.3847/2041-8213/aa72da](https://doi.org/10.3847/2041-8213/aa72da)
- Rothman, L. S., Gordon, I. E., Barbe, A., et al. 2009, *JQSRT*, 110, 533, doi: [10.1016/j.jqsrt.2009.02.013](https://doi.org/10.1016/j.jqsrt.2009.02.013)
- Rothman, L. S., Gordon, I. E., Barber, R. J., et al. 2010, *JQSRT*, 111, 2139, doi: [10.1016/j.jqsrt.2010.05.001](https://doi.org/10.1016/j.jqsrt.2010.05.001)
- Schwarz, G. 1978, *Annals of Statistics*, 6, 461
- Schweitzer, A., Hauschildt, P. H., Allard, F., & Basri, G. 1996, *MNRAS*, 283, 821, doi: [10.1093/mnras/283.3.821](https://doi.org/10.1093/mnras/283.3.821)
- Skilling, J. 2004, in *American Institute of Physics Conference Series*, Vol. 735, American Institute of Physics Conference Series, ed. R. Fischer, R. Preuss, & U. V. Toussaint, 395–405, doi: [10.1063/1.1835238](https://doi.org/10.1063/1.1835238)
- Ter Braak, C. J. F. 2006, *Statistics and Computing*, Volume 16, Issue 3, pp 239–249, 2006, 16, doi: [10.1007/s11222-006-8769-1](https://doi.org/10.1007/s11222-006-8769-1)
- ter Braak, C. J. F., & Vrugt, J. A. 2008, *Statistics and Computing*, 18, 435, doi: [10.1007/s11222-008-9104-9](https://doi.org/10.1007/s11222-008-9104-9)
- Waldmann, I. P., Tinetti, G., Rocchetto, M., et al. 2015, *ApJ*, 802, 107, doi: [10.1088/0004-637X/802/2/107](https://doi.org/10.1088/0004-637X/802/2/107)
- Welbanks, L., & Madhusudhan, N. 2019, *AJ*, 157, 206, doi: [10.3847/1538-3881/ab14de](https://doi.org/10.3847/1538-3881/ab14de)
- Wildt, R. 1939, *ApJ*, 90, 611, doi: [10.1086/144125](https://doi.org/10.1086/144125)
- Yurchenko, S. N., Bond, W., Gorman, M. N., et al. 2018, *MNRAS*, 478, 270, doi: [10.1093/mnras/sty939](https://doi.org/10.1093/mnras/sty939)
- Zahnle, K., Marley, M. S., Freedman, R. S., Lodders, K., & Fortney, J. J. 2009, *ApJL*, 701, L20, doi: [10.1088/0004-637X/701/1/L20](https://doi.org/10.1088/0004-637X/701/1/L20)